Journal of Asian Earth Sciences 257 (2023) 105838

Contents lists available at ScienceDirect

Journal of Asian Earth Sciences

journal homepage: www.elsevier.com/locate/jseaes

Hydrogen isotopic characteristics of shale gases

Yunyan Ni [a,*], Dazhong Dong [b], Limiao Yao [b], Jianping Chen [a], Jianli Sui [c], Fei Wang [d], Fei Liu [d], Jian Li [b], Jinhao Guo [b], Dan Liu [b], Jinliang Gao [b]

[a] China University of Petroleum (Beijing), Beijing 102249, China
[b] PetroChina Research Institute of Petroleum Exploration and Development, Beijing 100083, China
[c] Institute of Geology, China Earthquake Administration, Beijing 100029, China
[d] PetroChina Zhejiang Oilfield Company, Hangzhou 311100, China

ARTICLE INFO

Keywords:
Shale gas
Hydrogen isotope
Wufeng-Longmaxi
Isotopic reversal
Sichuan Basin

ABSTRACT

Sichuan Basin is important commercial shale gas producing basin in China, where shale gas explorations were mainly targeted at the Upper Ordovician Wufeng-Lower Silurian Longmaxi formations with burial depth mostly of 2000 ~ 3500 m. This study performed a detailed investigation about the δ^2H features of shale gases from the Wufeng-Longmaxi shale with burial depth of <2250 m (Taiyang), 2250 ~ 3500 m (Jiaoshiba) and >3500 m (Weirong). The average δ^2H_1 and δ^2H_2 values are of −135‰ and −146‰, −137‰ and −157‰, −137‰ and −124‰, respectively in Taiyang, Jiaoshiba and Weirong shale gas fields. The average δ^2H_1 values are nearly the same in the three gas fields, while average $\delta^{13}C_1$ values increase from −35.2‰ to −28.5‰ as from Weirong to Taiyang. When wetness >8%, δ^2H_1 values increase with decreasing wetness rapidly implying dominant influences from maturity, when wetness <8%, the δ^2H_1 variation is small and mainly in the range of (−140 ± 15)‰, indicating a strong influence from cogenetic water. All gases are characterized by a trend of $\delta^{13}C_1 > \delta^{13}C_2 > \delta^{13}C_3$, and gases in Taiyang and Jiaoshiba are characterized by $\delta^2H_1 > \delta^2H_2$, while gases in Weirong are dominated by $\delta^2H_1 < \delta^2H_2$. Generally, with decreasing gas wetness, ethane first become more enriched in D and ^{13}C, then become more depleted in D and ^{13}C, and finally become more enriched in D and ^{13}C again. The turning point of wetness from rollover to post-rollover zones is 1.2% for the $\delta^{13}C_2$ while 0.8% for the δ^2H_2. Such delay in δ^2H_2 also indicates the strong influences from the cogenetic water medium.

1. Introduction

Natural gas is the cleanest and least carbon green energy among the fossil fuels. With increasing demand for green energy, shale gas has attracted more and more attention. According to the empirical observations (Barker, 1984; Chen et al., 1995; Dai et al., 2005, 2012a; Schoell, 1980; Stahl, 1977), laboratory experiments (Behar et al., 1995; Berner and Faber, 1996; Lorant et al., 1998) and theoretical calculations (Chung et al., 1988; Ni et al., 2011; Rooney et al., 1995; Tang et al., 2000), it has long been considered that primary thermogenic gas is characterized by positive carbon and hydrogen isotopic distribution patterns among the C_1-C_3 alkanes ($\delta^{13}C_1 < \delta^{13}C_2 < \delta^{13}C_3$, $\delta^2H_1 < \delta^2H_2 < \delta^2H_3$). However, recent studies found that shale gas is often dominated by partial carbon isotopic reversal ($\delta^{13}C_1 > \delta^{13}C_2$, $\delta^{13}C_2 > \delta^{13}C_3$) or even complete carbon isotopic reversal ($\delta^{13}C_1 > \delta^{13}C_2 > \delta^{13}C_3$) (Dai et al., 2014, 2016; Feng et al., 2019; Hao and Zou, 2013; Rodriguez and Philp, 2010; Tilley and Muehlenbachs, 2013; Zumberge et al., 2012), or extremely heavy carbon isotopic values of methane (Feng et al., 2020; Ni et al., 2022a) at relatively high thermal maturity. A number of mechanisms such as mixing of primary and secondary products and water involved reactions have been invoked to account for such carbon isotopic anomaly (Dai et al., 2014; Feng et al., 2019; Hao and Zou, 2013; Rodriguez and Philp, 2010; Tilley and Muehlenbachs, 2013; Xia et al., 2013; Xia and Gao, 2018; Zumberge et al., 2012).

The hydrogen isotopic fractionation during gas generation is much greater than that of the carbon isotope, so compound-specific hydrogen isotope has been an attractive diagnostic tool in petroleum research (Ni et al., 2011). According to the few available studies related to the hydrogen isotope, it is found that hydrogen isotopic reversal between methane and ethane ($\delta^2H_1 > \delta^2H_2$) has also been observed in the deep non-associated gases from the northern Appalachian Basin (Burruss and Laughrey, 2010), and the post-mature Longmaxi shale gases in the Sichuan Basin (Dai et al., 2014). Pyrolytic experiment also documented a depletion in D of ethane at elevated temperatures (Ni et al., 2018a).

* Corresponding author.
E-mail address: niyunyan@cup.edu.cn (Y. Ni).

https://doi.org/10.1016/j.jseaes.2023.105838
Received 5 September 2022; Received in revised form 21 August 2023; Accepted 26 August 2023
Available online 28 August 2023

However, to date, no systematic study has been carried out on the shale gases to investigate the hydrogen isotopic fractionation and its differences from the carbon isotopic composition.

After a decade's effort, China has been the largest shale gas producer outside North America. It has made great achievements in the shale gas exploration with burial depths of 2000 ~ 3500 m and the annual shale gas production reached 240 × 10^8 m^3 in 2022. Recently, achievements have been made in the shallow (burial depth < 2250 m) and deep (burial depth > 3500 m) layers (Liang et al., 2020, 2021; Wang et al., 2019). In this study, gases from the Taiyang (burial depth < 2250 m), Jiaoshiba (burial depth of 2250 ~ 3500 m) and Weirong (burial depth > 3500 m) shale gas fields are compared to shale gases from other locations in the world. The major objective is to examine the hydrogen isotopic compositions of the shale gases and clarify the differences between carbon and hydrogen isotopes. This work will help to improve our understanding of the hydrogen isotopic fractionation and controlling factors, thus further improve our future interpretation of the hydrogen isotopic compositions of shale gases.

2. Geological settings

Sichuan Basin is one of the most stable sedimentary basins and the most important shale gas producing basin in China (Fig. 1). It has an area of around 180 × 10^3 km^2 and belongs to a large superimposed basin. It developed three sets of marine facies black shales including the Proterozoic Lower Sinian Doushantuo Formation, the Paleozoic Lower Cambrian Qiongzhusi Formation and the Upper Ordovician Wufeng-Lower Silurian Longmaxi formations (Fig. 2). Among them, the Wufeng-Longmaxi formations are the major commercial shale gas producing strata and a number of shale gas fields have been found.

The Wufeng-Longmaxi hot shale is deposited in a deep water shelf facies environment and has thickness of 80 ~ 120 m. It is dominated by Type I and Type II_1 kerogen and characterized by high TOC content (1.0% ~ 10.2%), relatively good porosity (1.7% ~ 10.9%) and permeability (0.01 ~ 44.4 × 10^{-3} mD). The burial depths of the Wufeng-Longmaxi shale differ greatly in different areas, covering shallow depths (<2250 m, i.e., Taiyang shale gas field), middle burial depths (2250 ~ 3500 m, i.e., Jiaoshiba shale gas field) and deep burial depths (>3500 m, i.e., Weirong shale gas field) (Fig. 1).

The Taiyang shale gas field, belonging to the Zhaotong national shale gas demonstration zone, is most famous for its shallow burial depths of the optimal reservoir section, i.e., 500 ~ 2250 m (Liang et al., 2020, 2021) (Table 1). It has been continuously uplifted since Late Jurassic and the uplift range reaches 2000 m. The Jiaoshiba shale gas field, belonging to the Fuling national shale gas demonstration zone, is the first shale gas field in China with annual shale gas production of 67 × 10^8 m^3 in 2020. Though the uplift in this area is also large and up to ~ 3000 m, the burial depths of optimal reservoir is mainly of 2250 ~ 3500

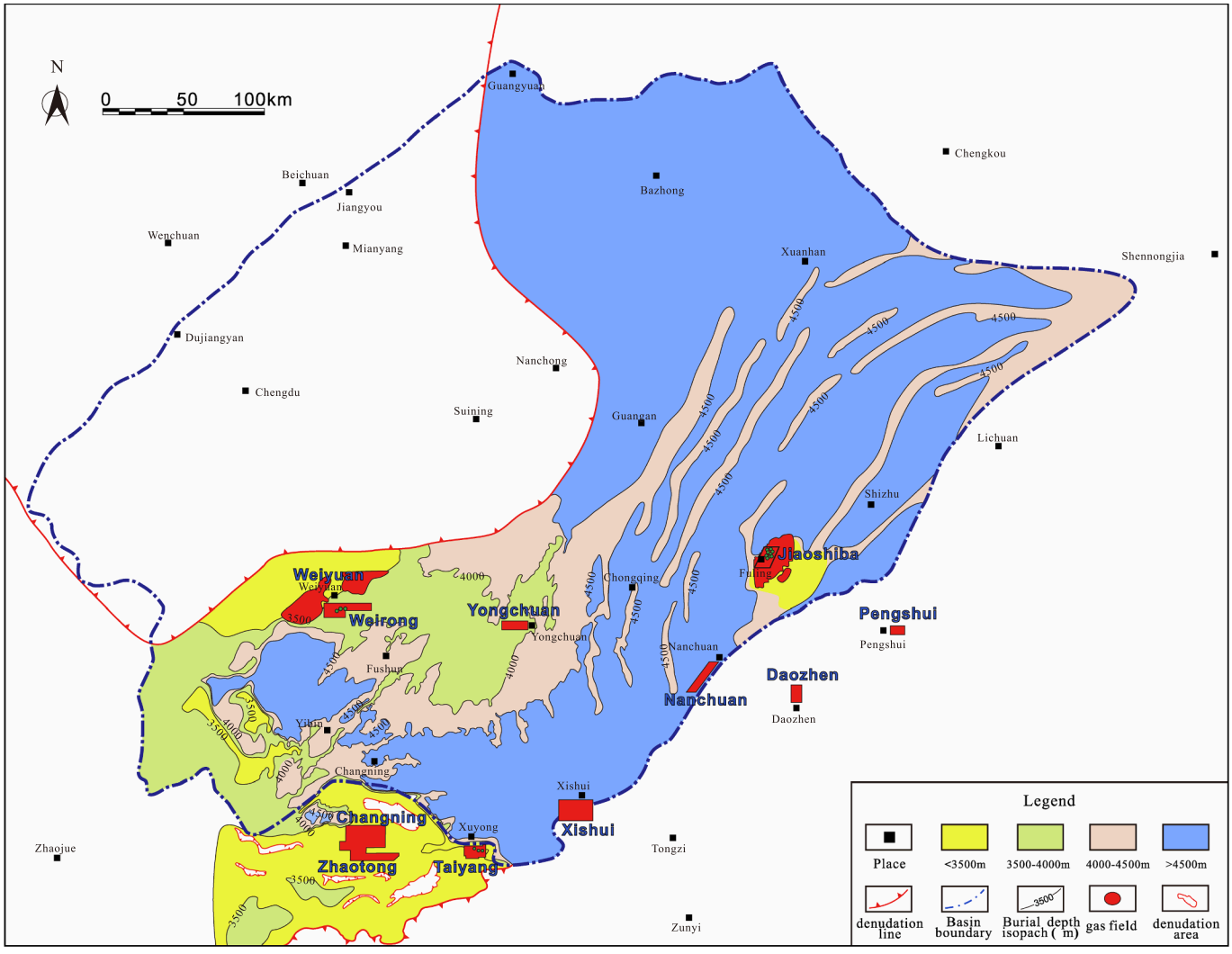

Fig. 1. Map showing the Taiyang, Jiaoshiba and Weirong shale gas fields and burial depths of the Upper Ordovician Wufeng-Lower Silurian Longmaxi formations in the Sichuan Basin (Ni et al., 2022a).

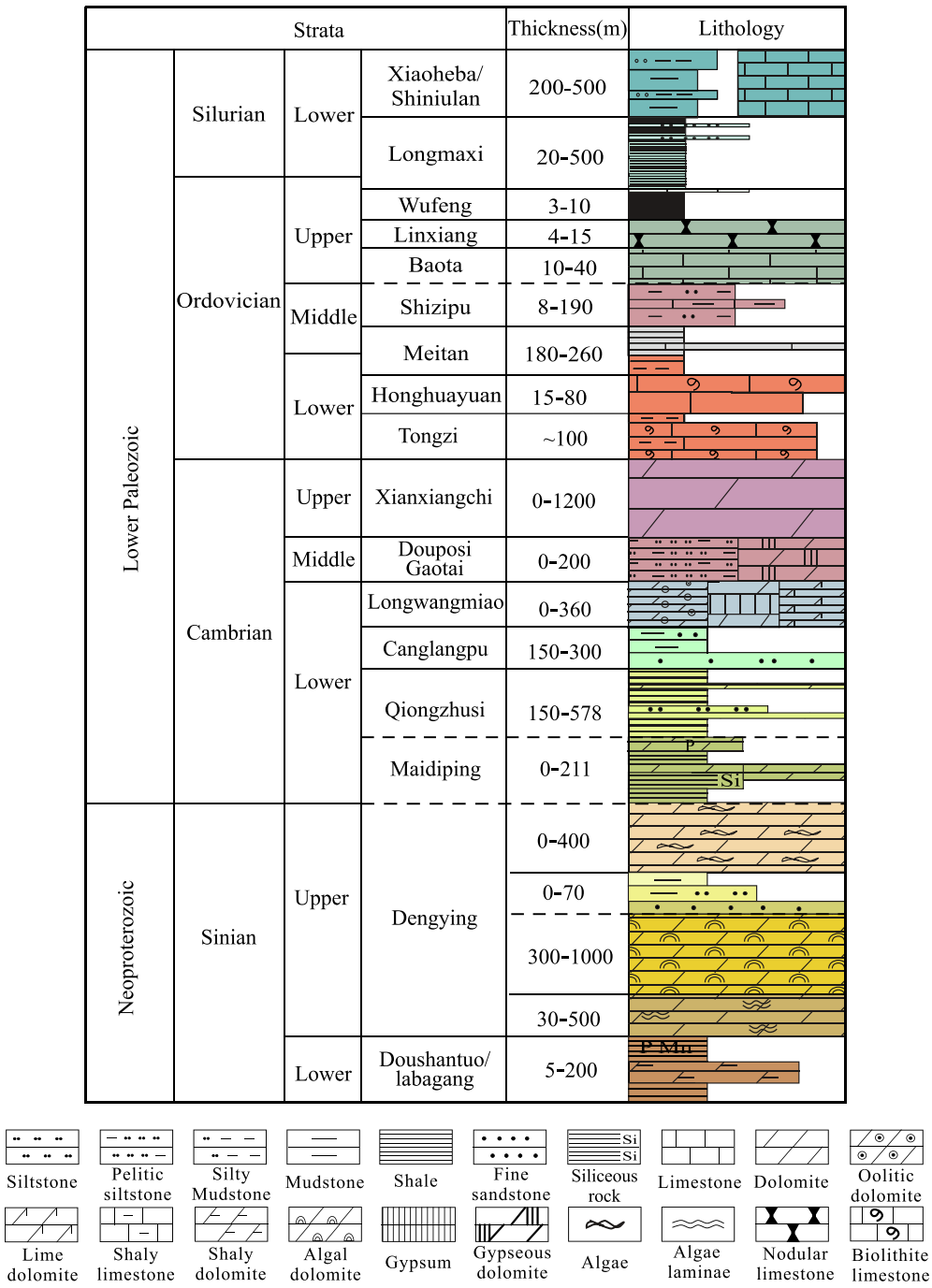

Fig. 2. Stratigraphic column of the Lower Paleozoic in the Sichuan Basin (modified from (Dai et al., 2016)).

Table 1
Geochemical information of the Taiyang, Jiaoshiba and Weirong shale gas fields.

Shale Gas Feld	Burial Depth m	Pressure Coefficient	Organic Matter	TOC %	Brittle Mineral %	Porosity %	Gas Production in 2020 $\times 10^8$ m^3
Taiyang	500–2250	1.2–1.47	Type II_1	0.42–9.05	55–70	2.92–8.01	4
Jiaoshiba	2250–3500	1.55	Type I	1.5–6.1	50–80	3.7–8.1	67
Weirong	3550–3880	1.94–2.06	Type I	2.8	64	6.07	

m. The Weirong shale gas field belongs to the Changning-Weiyuan national shale gas demonstration zone. In this area, structures are gentle and faults are not very developed. Though the Jurassic strata are exposed to the surface due to the basin uplift, burial depths of the optimal shale gas reservoirs are of 3550 ~ 3880 m. In general, the formation pressure coefficient is 1.2 ~ 1.47, 1.55, and 1.94 ~ 2.06 for Taiyang, Jiaoshiba and Weirong shale gas fields, respectively. the Taiyang shale gas field is dominated by Type II_1 organic matter with TOC content of 0.42%~9.05%, brittle mineral content of 55%~70%, porosity of 2.92%~8.01% and annual shale gas production of 4.0 $\times 10^8$

m^3 in 2020 (Liang et al., 2020, 2021; Ni et al., 2022a; Zou et al., 2021). The Jiaoshiba shale gas field is dominated by Type I organic matter with TOC of 1.5%~6.1%, pressure coefficient of 1.55, porosity of 3.7% ~8.1%, and brittle mineral content of 50%~80% (Dai et al., 2016; Zou et al., 2021). The Weirong shale gas field is dominated by Type I organic matter with TOC averagely of 2.8%, formation pressure coefficient of 1.94 ~ 2.06, porosity of 6.07%, and brittle mineral content of 64% (Ni et al., 2022a).

Due to the lack of effective calibration from vitrinite reflectance at very high maturation stage, determination of the exact thermal maturity of the Wufeng-Longmaxi shale is very difficult. According to the comparison with the section samples of the Wufeng-Longmaxi shale and the Permian coal samples in the Changning-Zhaotong areas (Ni et al., 2022a), the results by Wang et al. (2019) was used in this study (Fig. 3). The Wufeng-Longmaxi shale has undergone very high temperature and is at post-mature stage at present, for example, the Wufeng-Longmaxi shale has undergone maximum temperature up to 210 °C in the Jiaoshiba area (Tenger et al., 2017). The equivalent vitrinite reflectance of the Wufeng-Longmaxi shale reaches 4.62% in the southwestern Sichuan Basin, which was mainly due to the thermal effects from the Emeishan basalt (Wang et al., 2019). According to the equivalent vitrinite reflectance calculated from graptolite, the thermal maturity is up to 3.92% in the Taiyang area, around 3.6% in the Jiaoshiba area and around 2.77% in the Weirong area (Wang et al., 2019).

3. Samples and methods

11 gas samples from the Weirong shale gas field, 10 gas samples from the Taiyang shale gas field and 10 gas samples from the Jiaoshiba shale gas field were collected via the double-ended steel bottles (10 cm diameter about 1,000 cm^3 volume) directly from the wellheads or separators in the gas fields (Fig. 1). Details about the sample collection and the determination of the molecular and stable carbon isotopic compositions see Ni et al. (2022a).

Stable hydrogen isotopes were determined using a GC/ TC/IRMS mass spectrometer at the PetroChina Research Institute of Petroleum Exploration and Development (RIPED). It consists of a Trace GC Ultra gas chromatograph (GC) interfaced with a micropyrolysis furnace (1450 °C) in line with a Finnigan MAT253 isotope ratio mass spectrometer. Individual gas components were separated using a HP-PLOT Q column (30 m × 0.32 mm × 20 μm), and the carrier gas is helium with flow rate of 1.5 ml/min. Via high-temperature thermal conversion, all gases were cracked into H_2 and then be injected into the mass spectrometer. Methane used the split injection mode (1:7), ethane and

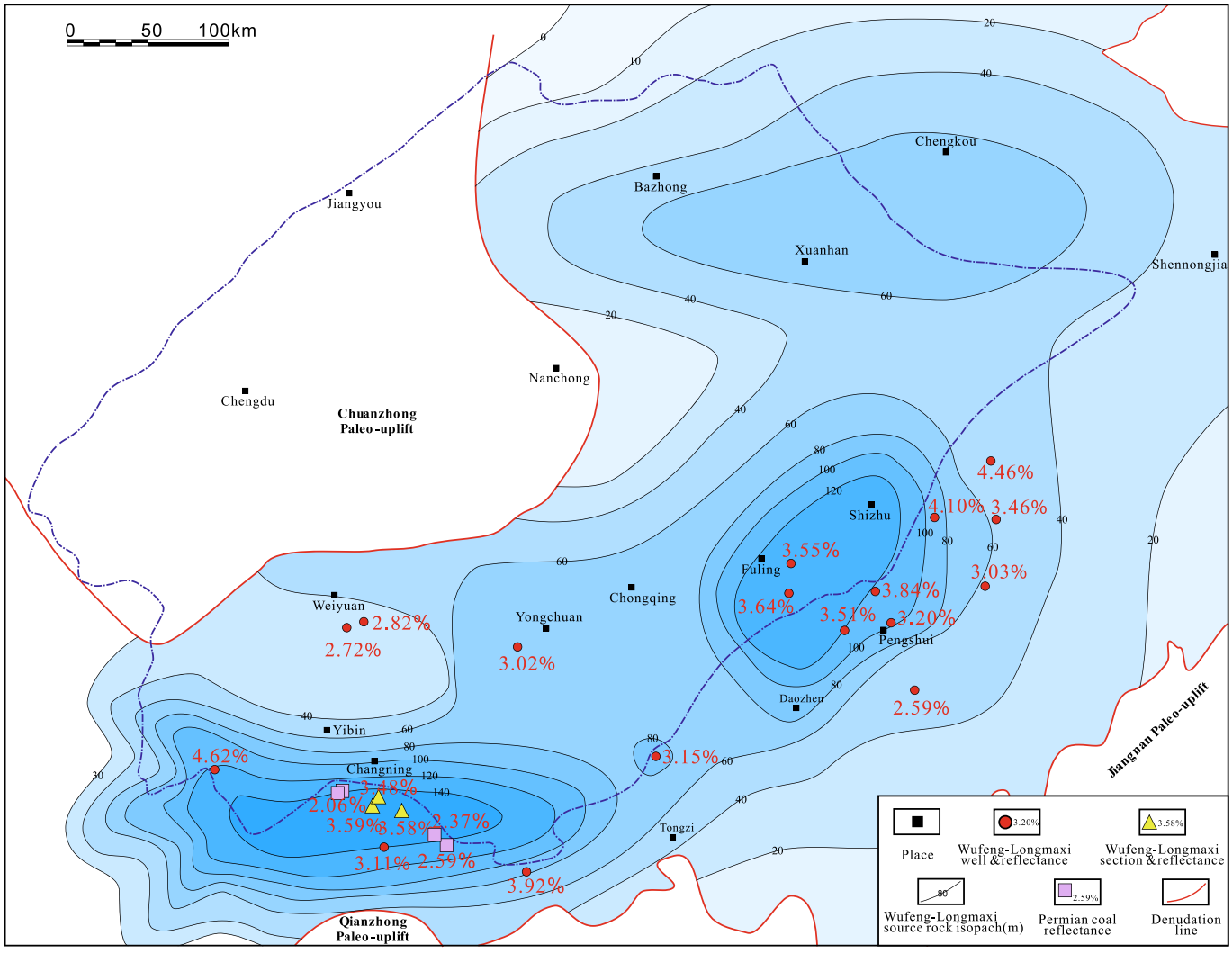

Fig. 3. Distribution map of the equivalent vitrinite reflectance of the Upper Ordovician Wufeng-Lower Silurian Longmaxi shale in the Sichuan Basin, China. Red circles are core samples of the Wufeng-Longmaxi shale (Wang et al., 2019), yellow triangles (section samples of the Wufeng-Longmaxi shale) and pink squares (Permian Longtan coal samples from coal mines) are for calibration (Ni et al., 2022a). Also shown are the thickness of the Upper Ordovician Wufeng-Lower Silurian Longmaxi black shale in Sichuan Basin. (For interpretation of the references to colour in this figure legend, the reader is referred to the web version of this article.)

propane used non-split injection mode. The temperature was at 40 °C for 4 min, increased to 80 °C at 10 °C/min, then to 140 °C at 5 °C/min, and finally reached 260 °C at 30 °C/min. The pyrolysis oven had temperature of 1450 °C. The stable hydrogen isotopic values (δ^2H) were reported in δ-notation in per mil (‰) relative to VSMOW and the precision is ± 3‰. Two laboratory working standards were used, i.e., one was a coal-derived hydrocarbon gas obtained from the Sulige gas field in the Ordos Basin and the other was an oil-related gas collected from the Tazhong gas field in the Tarim Basin, China. Both of them have been calibrated via two-point calibrations by ten laboratories carrying out>800 measurements including both on-line and off-line methods (Dai et al., 2012b).

In addition to the 31 collected gas samples, published data about the marine facies Wufeng-Longmaxi shale gases in the Changning-Weiyuan, Fuling and Zhaotong national shale gas demonstration zones, and Pengshui and Yongchuan areas in the Sichuan Basin in China (Cao et al., 2020; Chen et al., 2020; Dai et al., 2016; Feng et al., 2019, 2020; Zhang et al., 2018), and the marine facies Barnett shale gases in the Fort Worth Basin, the Fayetteville shale gases in the Arkoma Basin and the New Albany shale gases in the Illinois Basin were also compared (Rodriguez and Philp, 2010; Strąpoć et al., 2010; Zumberge et al., 2012).

4. Results

The $\delta^{13}C_1$, $\delta^{13}C_2$ and $\delta^{13}C_3$ values are of −29.5‰~-27.1‰ (average at −28.5‰, n = 10), −36.8‰~–33.7‰ (average at −35.4‰, n = 10) and −37.6‰~-34.6‰ (average at −36.2‰, n = 10), respectively for gases from the Taiyang shale gas field, of –32.7‰~-29.0 (average at −30.3‰, n = 10), −37.5‰~-35.5‰ (average at −36.4‰, n = 10) and −39.5‰~-37.7‰ (average at −38.4‰, n = 10), respectively for gases from the Jiaoshiba shale gas field and of −35.9‰~-34.1‰ (average at −35.2‰, n = 11), −39.7‰~-38.4‰ (average at −38.9‰, n = 11) and −42.0‰~-38.7‰ (average at −40.8‰, n = 11), respectively for gases from the Weirong gas field (Table 2) (Ni et al., 2022a).

Gases from the Taiyang, Jiaoshiba and Weirong shale gas fields have similar hydrogen isotopic composition of methane but very different hydrogen isotopic composition of ethane (Table 2). Gas samples from the Taiyang gas field have δ^2H_1 values of −140‰ ~ −129‰ with an average of −135‰ (n = 10), gas samples from the Jiaoshiba gas field have δ^2H_1 values of −141‰ ~ −135‰ with an average of −137‰ (n = 10), and gas samples from the Weirong gas field have δ^2H_1 values of −139‰ ~ −136‰ with an average of −137‰ (n = 11) (Table 2). The Wufeng-Longmaxi shale in southern Sichuan Basin is mostly at post-mature stage, and the equivalent vitrinite reflectance based on graptolite is up to 3.92% in the Taiyang area, around 3.60% in the Jiaoshiba area and about 2.77% in the Weirong area (Wang et al., 2019). Though the maturity changes from 2.77% (Weirong) to 3.92% (Taiyang), δ^2H values of methane are very similar, with a total variation of 12‰ in the three gas fields and an average of −137‰ in both Jiaoshiba and Weirong gas fields and −135‰ in Taiyang gas field. In comparison, the Fayetteville shale gas, which has slightly lower gas maturity (Ro = 2.0%–3.0%), has similar average δ^2H_1 values of −133‰ (n = 101), even they have relatively large variation, −153‰ ~ −123‰ (Zumberge et al., 2012). The Barnett shale gas, which has further lower gas maturity (Ro = 1.0%–2.0%), shows much larger variation of δ^2H_1 values, i.e., −215‰ ~ −101‰ with an average of −147‰ (n = 164) (Rodriguez and Philp, 2010; Zumberge et al., 2012). The New Albany shale gas, with gas maturity of 0.7% in the Pike County, has δ^2H_1 values of −254‰ ~ −216‰ with an average of −237‰ (Strąpoć et al., 2010).

In contrast to the similar δ^2H_1 values in the three gas fields, δ^2H_2 values have large variation. Gas samples from Taiyang gas field have δ^2H_2 values of −154‰ ~ −137‰ with an average of −146‰ (n = 10), gas samples from the Jiaoshiba gas field have δ^2H_2 values of −164‰ ~ −153‰ with an average of −157‰ (n = 10), and gas samples from the Weirong gas field have δ^2H_2 values of −128‰ ~ −118‰ with an average of −124‰ (n = 11) (Table 2). In comparison, the Barnett shale

Table 2
Hydrogen isotopic compositions of gases. Molecular and carbon isotopic compositions are from (Ni et al., 2022a). The gas maturity (Ro%) was calculated according to the formula by Chen et al. (2021).

Gas Field	Well	well depth	burial depth	Composition (%)					$\delta^{13}C$ (‰)			δ^2H (‰)		Ro%
		m	m	CH_4	C_2H_6	C_3H_8	CO_2	N_2	CH_4	C_2H_6	C_3H_8	CH_4	C_2H_6	Chen et al. (2021)
Taiyang	Yang102 H2-2	2204.86	919.9	98.81	0.60	0.01		0.58	−29.5	−36.2	−37.0	−133	−154	3.31
	Yang102 H2-6	2275.24	969.95	98.88	0.63	0.01		0.48	−29.4	−36.6	−37.6	−140	−150	3.34
	Yang102 H2-8	2589.82	995.82	99.03	0.66	0.01		0.30	−29.5	−36.8	−37.0	−135	−147	3.31
	Yang105 H2-8	2300	1249.86	99.01	0.48	0.01		0.50	−28.7	−36.0	−36.5	−135	−152	3.56
	Yang105 H2-6	2285	1414.845	98.76	0.49	0.01		0.45	−29.1	−35.4	−37.1	−133	−145	3.45
	Yang105 H2-4	2400	1501.065	98.88	0.53	0.01	0.05	0.52	−29.1	−35.9	−36.3	−135	−148	3.43
	Yang105 H2-2	2300	1544.28	98.94	0.57	0.02	0.05	0.40	−28.4	−35.7	−36.3	−129	−137	3.66
	Yang105 H3-6	3325	2059.13	98.50	0.71	0.11	0.13	0.41	−27.2	−34.3	−34.8	−133	−141	4.08
	Yang105 H3-4	3390	2140.76	98.88	0.59	0.01	0.14	0.37	−27.2	−33.7	−34.6	−134	−144	4.08
	Yang105 H3-2	3426	2245.66	98.57	0.59	0.01	0.15	0.67	−27.1	−33.7	−34.9	−137	−141	4.12
Jiaoshiba	JY1-2HF	4168	2416.215	98.09	0.62	0.03	0.31	0.84	−30.3	−35.5	−37.7	−140	−157	3.1
	JY2-3HF	4518	2479.58	98.23	0.63	0.02	0.31	0.81	−29.0	−35.7	−38.1	−136	−154	3.5
	JY3-3HF	3561	2428.855	97.98	0.61	0.02	0.35	0.95	-32.7	−37.5	−38.2	−141	−164	2.5
	JY4-2HF	4312	2598.44	98.21	0.56	0.01	0.44	0.77	−30.2	−36.5	−38.2	−136	−159	3.1
	JY56-2HF	4498	2818.265	98.09	0.52	0.01	0.57	0.81	−29.4	−36.1	−38.0	−137	−162	3.3
	JY18-5HF	4650	2820.685	98.14	0.53	0.02	0.34	0.96	−30.0	−36.5	−38.9	−136	−156	3.2
	JY9-6HF	4147	2310.17	98.26	0.64	0.02	0.21	0.87	−30.0	−36.2	−38.5	−136	−159	3.2
	JY39-7HF	5410	2778.295	98.18	0.63	0.02	0.37	0.81	−30.4	−36.8	−39.5	−135	−153	3.0
	JY37-6HF	5865	3139.72	98.09	0.47	0.01	0.60	0.83	−30.1	−36.6	−39.2	−137	−154	3.1
	JY61-2HF	4770	3037.515	98.01	0.45	0.01	0.66	0.88	−30.3	−36.9	−38.1	−139	−153	3.1
Weirong	WY29-1HF	5430	3743	97.66	0.46	0.02	1.26	0.60	−35.4	−39.3	−41.9	−137	−122	1.9
	WY29-2HF	5390	3737	97.70	0.50	0.02	1.20	0.58	−35.9	−39.3	−42.0	−139	−124	1.8
	WY29-4 + 5 + 6		3690	97.76	0.50	0.02	1.19	0.52	−35.4	−39.7	−41.8	−137	−122	1.9
	WY23-4HF	5546	3800	97.42	0.44	0.02	1.64	0.49	−35.2	−38.8	−41.1	−138	−118	2.0
	WY23-2HF	5600	3830.22	97.23	0.42	0.01	1.72	0.61	−34.9	−38.4	−40.8	−137	−123	2.0
	WY23-6HF	5596	3831.96	97.41	0.43	0.01	1.66	0.48	−34.9	−38.5	−40.7	−137	−120	2.0
	WY43-1HF	5520	3720	91.91	0.19	0.00	6.64	1.25	−34.1	−38.6	−38.8	−137	−127	2.2
	WY43-2HF	5540	3737	96.37	0.46	0.02	2.76	0.38	−35.1	−38.9	−38.9	−136	−126	2.0
	WY43-3HF	5585	3744	97.40	0.48	0.03	1.59	0.49	−35.6	−38.6	−38.7	−138	−128	1.9
	WY43-4HF	5595	3778	97.55	0.46	0.02	1.53	0.44	−35.4	−38.7	−41.9	−136	−126	1.9
	WY43-5HF	5610	3770	97.58	0.47	0.02	1.38	0.55	−35.4	−39.1	−42.0	−138	−124	1.9

gas has δ^2H_2 values of −153‰ ~ −94‰ with an average of −126‰ (n = 40) (Rodriguez and Philp, 2010) and the New Albany shale gas has δ^2H_2 values of −335‰ ~ −273‰ with an average of −303‰ (Strąpoć et al., 2010).

5. Discussion

5.1. Hydrogen isotopic anomaly of methane

Previous study found that both carbon and hydrogen isotopic compositions of methane have a linear logarithmic relationship with the thermal maturity (Ro%) of precursor organic matter, so both carbon and hydrogen isotopic composition of methane should increase with increasing thermal maturity (Schoell, 1980). Though gases from Taiyang, Jiaoshiba and Weirong gas fields show clear carbon isotopic reversal between methane and ethane ($\delta^{13}C_1 > \delta^{13}C_2$), both methane and ethane have comparative carbon isotopic variation with increasing thermal maturity from Weirong gas field to Taiyang gas field, i.e., when the maturity changes from 2.77% in Weirong gas field to 3.92% in Taiyang gas field, the variation is 8.8‰ for $\delta^{13}C_1$ values and 6.0‰ for $\delta^{13}C_2$ values, and a good linear correlation exists between $\delta^{13}C_1$ and $\delta^{13}C_2$ values (R^2 = 0.9229) (Fig. 4a). In contrast, only gases from Taiyang and Jiaoshiba gas fields have hydrogen isotopic reversal between methane and ethane ($\delta^2H_1 > \delta^2H_2$), and gases from Weiyuan gas field are characterized by $\delta^2H_1 < \delta^2H_2$. Moreover, when the maturity changes from 2.77% in Weirong gas field to 3.92% in Taiyang gas field, the variation of $\delta^2H_1 <$ is only 12‰, while the variation of δ^2H_2 reaches 46‰, which is nearly four times that of the δ^2H_1 values (Fig. 4b). Unlike the carbon isotope, there is no linear correlation between δ^2H_1 and δ^2H_2 values. Actually, gas samples from the Taiyang, Jiaoshiba and Weirong shale gas fields have nearly the same average δ^2H_1 values, i.e., the average δ^2H_1 value is −137‰ for the gases in Jiaoshiba and Weirong gas fields and −135‰ for the gases in Taiyang gas field.

The ^{13}C concentration in methane is mainly dependent on the thermal maturity and the type of source organic matter (Dai, 1993; Schoell, 1980; Stahl and Carey, 1975; Tang et al., 2000). However, the D concentration in methane is not only affected by the thermal maturity of source organic matter, but also influenced by the water salinity of the depositional environment of source organic matter (Huang et al., 2019; Ni et al., 2019; Schoell, 1980; Wang et al., 2015a). In summary, hydrogen isotope of hydrocarbon gases increases with increasing water salinity of the depositional environment of source rocks and the thermal maturity of source rocks (Huang et al., 2019; Ni et al., 2019; Schoell, 1980; Wang et al., 2015a). Shale from these three gas fields were all deposited in the environment of deep saline water shelf facies. At the Silurian Rhuddanian stage, water salinity should be similar in these three areas. However, in the Silurian Aeronian stage, sea closure in the Sichuan Basin was enhanced, resulting in the increase of water salinity. While the ocean opening was in the Chengkou-Shennongjia area in the northern basin (Fig. 1), so Jiaoshiba area is close to the ocean opening in the northern basin and should have relatively weak sea closure effect and slightly lower water salinity (Wang et al., 2015b, 2018). In general, there is no big difference of water salinity in these three areas, which can be well reflected in the hydrogen isotopic values of methane. From Taiyang to Weirong, the thermal maturity changes from ~ 3.92% in Taiyang to ~ 3.60% in Jiaoshiba, and finally to ~ 2.77% in Weirong (Wang et al., 2019), methane becomes more and more depleted in ^{13}C, but nearly constant in D (Fig. 4). This clearly demonstrates the important impacts from the water salinity of the depositional environment, and similar water salinity in these areas results in the similar hydrogen isotopic values in methane. It agrees well with the results by Ni et al. (Ni et al., 2019) that water salinity of the depositional environment has very strong influences on the hydrogen isotopes.

At temperature of 200 °C, an isotopic equilibrium was achieved between CH_4 and H_2O, and the δ^2H values of methane will be about 65‰ lower than that of the cogenetic water (Bottinga, 1969). Oilfield water which is associated with natural gas generally has δ^2H values of (-25 ± 15)‰, so methane in equilibrium with these waters should have δ^2H values of −75‰ to −105‰, and lower temperatures will result in more positive δ^2H values (Schoell, 1980). In the southern Sichuan Basin, the hydrous hydraulic flowback/produced water of the Wufeng-Longmaxi shale gas has δ^2H values of –23.9‰ (n = 67) in the Weiyuan area and −28.2‰ (n = 35) in the Changning area (Ni et al., 2018b, 2022b). Here flowback water is referred to the water that returns to the surface after the hydraulic fracturing process is complete, and produced water is referred to the water that is extracted together with shale gas during production (Vengosh et al., 2014). Previous study proposed that the flowback/produced water is composed of injected water and saline brine of the hosted shale formation, and the high-salinity brine endmember of the Wufeng-Longmaxi shale gas flowback/produced water has similar composition with the Cambrian formation water which has δ^2H values up to −25.6‰ (Ni et al., 2018b, 2022b). Methane in equilibrium with formation brines should have δ^2H values of about −90‰ for the Wufeng-Longmaxi shale gas. However, the Wufeng-Longmaxi shale gases from Taiyang, Jiaoshiba and Weirong shale gas fields have δ^2H_1 values of −136‰ (n = 31). To some extent, this should indicate that hydrogen isotopic equilibrium has not been achieved between methane and associated waters though the Wufeng-Longmaxi shale has experienced maximum temperatures up to 210 °C (Tenger et al., 2017). Laboratory experimental results may not support that CH_4-H_2O hydrogen exchange can be the main contribution to the δ^2H_1 values. Recent experimental study found extensive and reversible D/H exchange between water and

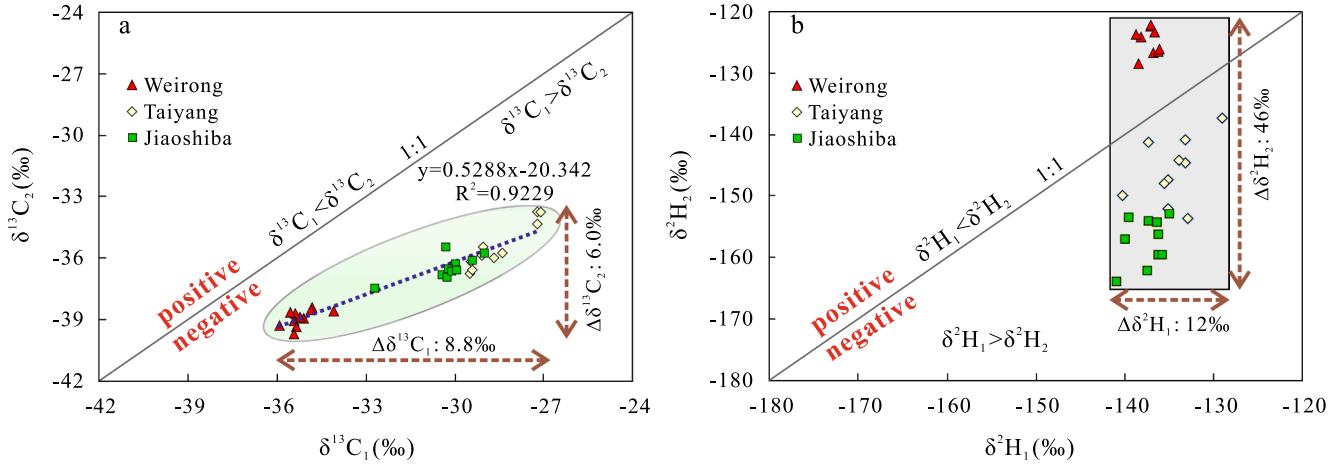

Fig. 4. $\delta^{13}C_1$ versus $\delta^{13}C_2$ (a) and δ^2H_1 versus δ^2H_2 (b) cross-plots of gases from Taiyang, Jiaoshiba and Weirong shale gas fields in the Sichuan Basin.

low-molecular C_2–C_5 n-alkanes at elevated temperatures and pressures on timescales of months, but comparatively minor exchange for CH_4 (Reeves et al., 2012). However, numerous studies have demonstrated the D/H exchange between sedimentary organic matter and ambient water at elevated temperatures and a pseudoequilibrium D/H fractionation of about −80‰ ~ −110‰ was suggested for the natural petroleum system (Schimmelmann et al., 2006). As shown in Fig. 5, when $\delta^{13}C_1$ < -42‰, δ^2H_1 values increase rapidly, while when $\delta^{13}C_1$ > -42‰, δ^2H_1 values change in a very small range, i.e., when $\delta^{13}C_1$ values change from around −54‰ to around −42‰ ($\Delta\delta^{13}C_1$ = 12‰), correspondingly the δ^2H_1 values change from around −260‰ to around −140‰ ($\Delta\delta^2H_1$ = 120‰); while when $\delta^{13}C_1$ values change from around −42‰ to around −24‰ ($\Delta\delta^{13}C_1$ = 18‰), correspondingly the δ^2H_1 values change from around −170‰ to around −130‰ ($\Delta\delta^2H_1$ = 40‰). During the thermal maturation, δ^2H values of sedimentary organic matter often increase systematically with thermal maturity, and the increase is the greatest when the difference between δ^2H values of water and sedimentary organic matter is the largest, and is the minimal when the difference between δ^2H values of water and sedimentary organic matter is 80‰–110‰ (Schimmelmann et al., 2006). The Wufeng-Longmaxi shale has experienced maximum temperatures up to 210 °C (Tenger et al., 2017) and the Barnett shale has experienced maximum temperatures up to 149 °C (Curtis, 2002). When $\delta^{13}C_1$ < -42‰, the thermal maturity is relatively low, and the difference between δ^2H values of water and sedimentary organic matter is relatively large, so the increase of the δ^2H values of sedimentary organic matter with increasing thermal maturity is relatively large, resulting in the rapid increase of δ^2H_1 values with increasing $\delta^{13}C_1$ values; when $\delta^{13}C_1$ > -42‰, the thermal maturity is relatively high, and a pseudoequilibrium D/H fractionation is achieved, so the increase of the δ^2H values of sedimentary organic matter with increasing thermal maturity is minimal, resulting in the nearly constant δ^2H_1 values with increasing $\delta^{13}C_1$ values (Fig. 5).

Such strong influences from cogenetic water on hydrogen isotope can also be seen in Fig. 6. When the burial depth increases from ~ 900 m to 2300 m, the $\delta^{13}C_1$, $\delta^{13}C_2$, $\delta^{13}C_3$ values increase by around 3‰, and good linear correlation between $\delta^{13}C$ values and burial depths exist for methane (R^2 = 0.9223), ethane (R^2 = 0.9252) and propane (R^2 = 0.888) (Fig. 6a). Generally thermal maturity increases with increasing burial depth. According to Well Wei28 in the Southern Sichuan, the vitrinite reflectance Ro% is 1.47% at burial depth of 926 m, and the Ro% value increases to 2.39% when the burial depth increases to 2537 m, so the increase of Ro% is 0.92 when burial depth increases from 926 m to 2537 m (Zhu et al., 2016). Based on the carbon isotope of methane, using the $\delta^{13}C_1$-Ro% formula by Chen et al. (2021), the calculated gas maturity of Ro% is 3.31% at burial depth of 920 m and increases to 4.12% at burial depth of 2246 m, so the increase of Ro% is 0.81% when burial depth increases from 920 m to 2246 m. This calculated increase of thermal maturity with burial depth is very similar to that determined from the field samples from Well Wei28, which demonstrates that thermal maturity is a very important factor causing the increase in carbon isotope of hydrocarbon gases with burial depth. However, if thermal maturity is the only factor that matters, one should see good correlation between $\delta^{13}C_1$ and Δ ($\delta^{13}C_2 - \delta^{13}C_1$), however, this is not the case. Hence, factor other than thermal maturity such as diffusive migration of gases can not be ignored. Because ^{12}C–^{12}C bonds are weaker than ^{12}C–^{13}C bonds and react faster, when upward diffusive migration occurs, methane in the shallow formation will be more enriched in ^{12}C compared to the source (Pernaton et al., 1996; Zhang and Krooss, 2001). Similarly, when upward diffusive migration occurs, the separates will be more enriched in CH_4 and depleted in ^{13}C and D, while the residual will be more depleted in CH_4 and enriched in ^{13}C and D. However, unlike the carbon isotopic compositions of methane, ethane and propane, there is no linear relationship between hydrogen isotopic compositions of methane and burial depths (R^2 = 0.0155), neither as ethane (R^2 = 0.5029) (Fig. 6b). Due to the strong influences from the associated water, δ^2H values of methane are relatively constant and impacts from both thermal maturity and diffusive migration are minimal, resulting in the extremely low correlation coefficient (R^2 = 0.0155).

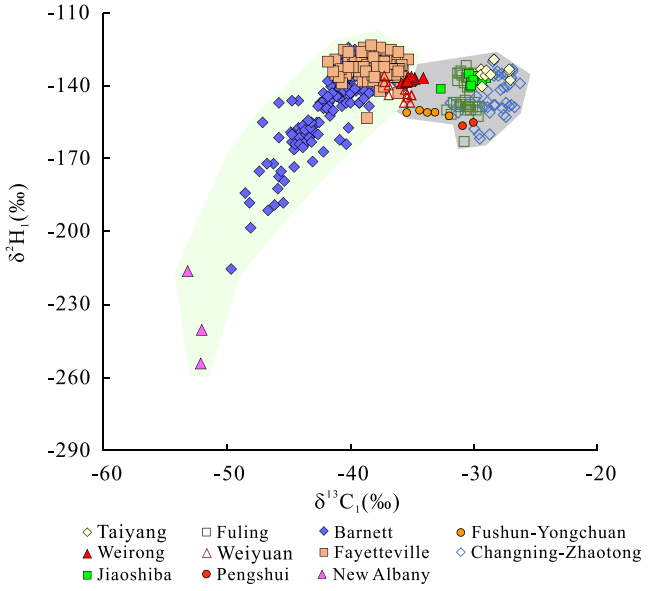

Fig. 5. Plot showing the $\delta^{13}C_1$ vs. δ^2H_1 of gases from the Taiyang, Jiaoshiba, and Weirong shale gas fields. Also shown are published data of the shale gases (Cao et al., 2020; Chen et al., 2020; Dai et al., 2016; Feng et al., 2019, 2020; Rodriguez and Philp, 2010; Strąpoć et al., 2010; Zhang et al., 2018; Zumberge et al., 2012).

5.2. Hydrogen isotopic distribution pattern

A number of studies have demonstrated that thermogenic gas which has not undergone post-genetic processes is normally characterized by positive carbon and hydrogen isotopic trend between methane, ethane and propane ($\delta^{13}C_1 < \delta^{13}C_2 < \delta^{13}C_3$, $\delta^2H_1 < \delta^2H_2 < \delta^2H_3$) (Barker, 1984; Chen et al., 1995; Dai, 1993; Dai et al., 2012a; Ni et al., 2013, 2015). This is due to the kinetic isotopic fractionation effect on kerogen/oil cracking reactions during decomposition processes. When an alkyl is separated from the source organic matter, ^{12}C–^{12}C or ^{12}C-H bonds are weaker than ^{12}C–^{13}C or ^{13}C-H bonds and react faster, so the residual high-molecular-weight source organic matter will be more enriched in ^{13}C compared to the low-molecular-weight product and thus result in the positive carbon isotopic trend ($\delta^{13}C_1 < \delta^{13}C_2 < \delta^{13}C_3$) (Lorant et al., 1998; Tang et al., 2000). Similarly, during the decomposition, ^{12}C–^{12}C bonds in all-^1H molecules have a lower activation energy and are easier to break than those in molecules containing at least one D, therefore, the residual high-molecular-weight source organic matter will be more enriched in D compared to the low-molecular-weight product, causing the positive hydrogen isotopic trend ($\delta^2H_1 < \delta^2H_2 < \delta^2H_3$) (Ni et al., 2011; Tang et al., 2005; Xia and Gao, 2017).

The Wufeng-Longmaxi gas samples from Taiyang, Jiaoshiba and Weirong gas fields are all characterized by negative carbon isotopic trend ($\delta^{13}C_1 > \delta^{13}C_2 > \delta^{13}C_3$), however, hydrogen isotopic reversal between methane and ethane only occurs in the Taiyang and Jiaoshiba gas fields ($\delta^2H_1 > \delta^2H_2$) (Fig. 7). Gas samples from Weirong gas field are characterized by negative carbon isotopic trend ($\delta^{13}C_1 > \delta^{13}C_2 > \delta^{13}C_3$) but positive hydrogen isotopic trend ($\delta^2H_1 < \delta^2H_2$) (Fig. 7). Compared to Taiyang and Jiaoshiba, the Wufeng-Longmaxi shale in the Weirong gas field has slightly lower maturity of 2.77% (Fig. 3), which might be a controlling factor on the positive hydrogen isotopic trend.

Previous studies have already demonstrated that depletion of ^{13}C in ethane and propane widely occurs in both field gas samples (Burruss and Laughrey, 2010; Dai et al., 2014, 2016; Feng et al., 2019 Jenden et al., 1993; Rodriguez and Philp, 2010; Tilley and Muehlenbachs, 2013;

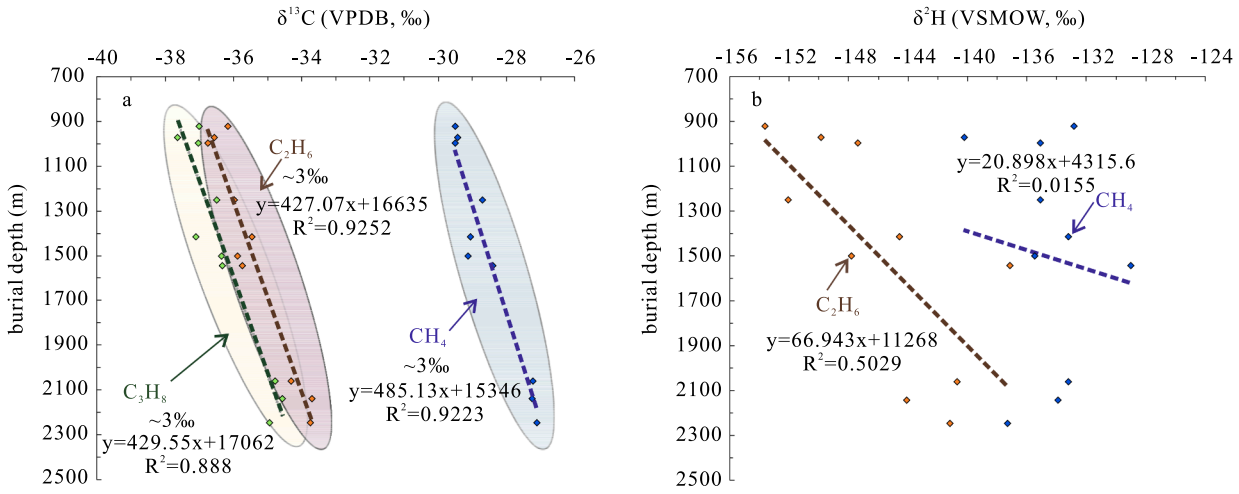

Fig. 6. Plots showing $\delta^{13}C_1$ versus burial depth (a) and $\delta^{2}H_1$ versus burial depth (b) of gases from the Taiyang, Jiaoshiba and Weirong shale gas fields in the Sichuan Basin, China. The $\delta^{13}C_1$ versus burial depth plot is from (Ni et al., 2022a).

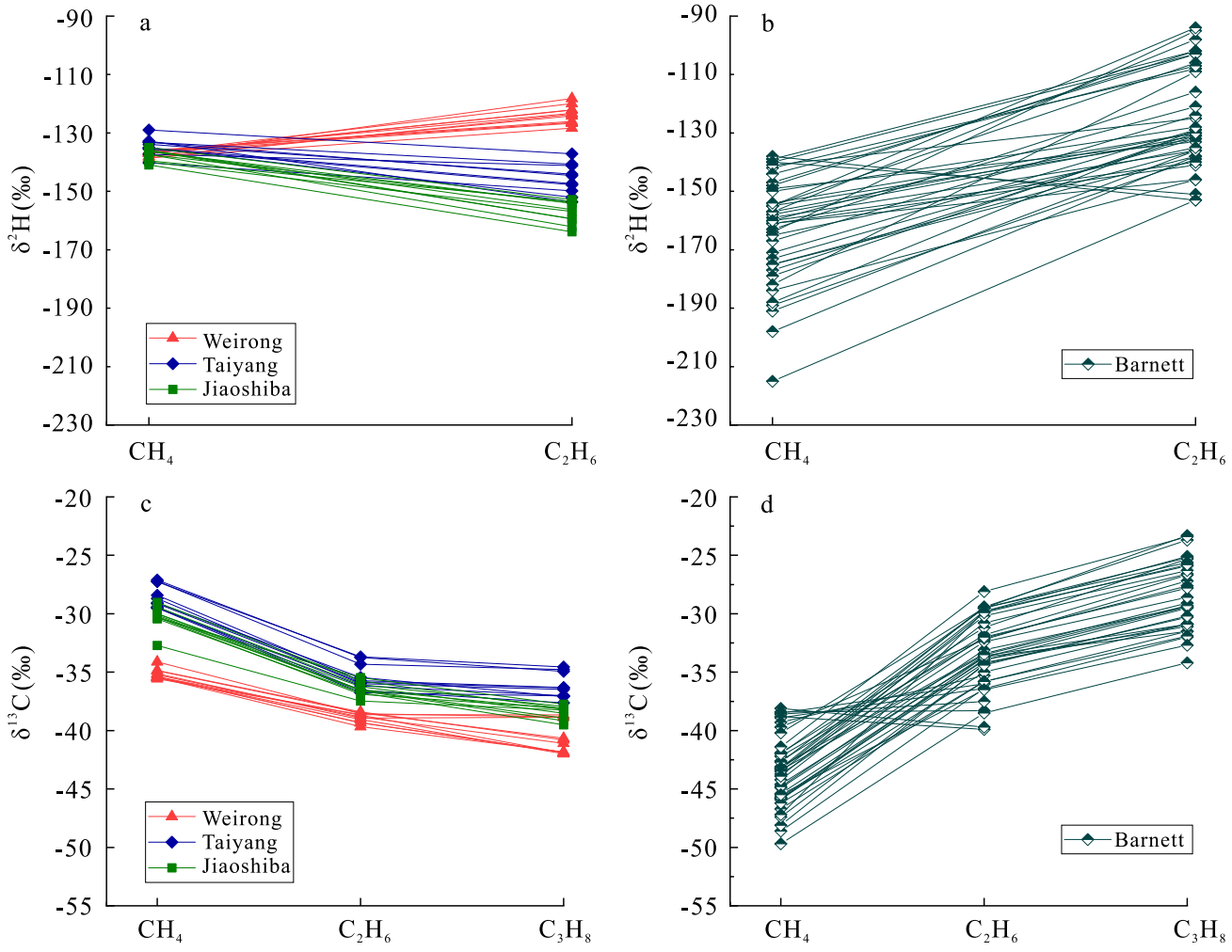

Fig. 7. Stable hydrogen isotopic composition of methane and ethane from the Wufeng-Longmaxi shale in Taiyang, Jiaoshiba and Weirong gas fields in the Sichuan Basin (a) and from Barnett shale in the Fort Worth Basin (b). Also shown are carbon isotopic compositions of methane, ethane and propane from the Wufeng-Longmaxi shale in Taiyang, Jiaoshiba and Weirong gas fields in Sichuan Basin (c) and from Barnett shale in the Fort Worth Basin (d). The carbon isotopic data of the Wufeng-Longmaxi shale gases are from (Ni et al., 2022a) and the carbon and hydrogen isotopic data of Barnett shale gases are from (Rodriguez and Philp, 2010).

Zumberge et al., 2012) and also in gaseous products during pyrolytic experiments (Gao et al., 2014; Ni et al., 2018a), which are apparently correlated with the high thermal maturity. The Barnett shale has equivalent vitrinite reflectance of 1.0%~2.0%, the shale gas is dominated by both positive carbon and hydrogen isotopic trends ($\delta^{13}C_1 < \delta^{13}C_2 < \delta^{13}C_3$, $\delta^2H_1 < \delta^2H_2$), and only the few samples with high gas maturity are characterized by the depletion of ^{13}C or D in ethane and/or propane (Rodriguez and Philp, 2010; Zumberge et al., 2012). The Fayetteville shale has equivalent vitrinite reflectance of 2.0%~3.0%, and the shale gas is characterized by partial or complete negative carbon isotopic trends ($\delta^{13}C_1 > \delta^{13}C_2 < \delta^{13}C_3$ or $\delta^{13}C_1 > \delta^{13}C_2 > \delta^{13}C_3$) (Zumberge et al., 2012). The Wufeng-Longmaxi shale has even higher equivalent vitrinite reflectance (>2.0%, up to 4.62%) (Wang et al., 2019), and the shale gas is also characterized by complete negative carbon isotopic trends (Dai et al., 2014, 2016; Feng et al., 2019; Ni et al., 2022a). It is clear that the carbon isotopic distribution pattern changes from positive normal trend to partial reversal trend and finally to complete reversal trend with increasing thermal maturity. Moreover, such changes of carbon isotopic distribution pattern not only occur in the marine facies shale gases originated from Type I and Type II_1 source organic matters, but also occur in the coal-derived thermogenic gases originated from Type III source organic matters (Dai et al., 2017). In the Ordos Basin, thermal maturity increases from northern basin to southern basin, and the carbon isotopic distribution pattern also changes from positive trend to partial reversal trend and finally into complete reversal trend (Fig. 8). Pyrolytic experiments on low mature type II kerogen (0.7% Ro%) also found that methane and ethane become depleted in ^{13}C after thermal maturity of 1.49% under hydrous conditions (Gao et al., 2014). Moreover, pyrolytic experiments on coal samples (0.62% Ro%) at constant temperatures for about 72 h demonstrated that ethane starts to be depleted in ^{13}C at 500 °C and be depleted in D at 450 °C, and propane starts to be depleted in ^{13}C at 450 °C, no matter with or without added water (Ni et al., 2018a). Therefore, high thermal maturity or high temperature plays a key role in both carbon and hydrogen isotopic distribution pattern.

Hydrogen isotopic composition of natural gases are mainly affected by the thermal maturity of the source rocks and the water salinity of the depositional environment of source rocks (Dai et al., 2012a; Liu et al., 2019; Ni et al., 2019; Schoell, 1980; Wang et al., 2015a), so under geological conditions, hydrogen isotopic distribution pattern might be more complex than that of the carbon isotope. Fig. 9 dynamically displays the hydrogen isotopic changes of ethane with increasing thermal maturity. At Ro% around 2.77% in the Weirong area, the hydrogen isotopic trend is positive between methane and ethane, i.e., $\delta^2H_1 < \delta^2H_2$; when Ro% reached 3.02% in the Yongchuan area, the hydrogen isotopic trend is still positive between methane and ethane, i.e., $\delta^2H_1 < \delta^2H_2$; when Ro% reached 3.20% in Pengshui area, the hydrogen isotopic trend becomes negative between methane and ethane, i.e., $\delta^2H_1 > \delta^2H_2$; when Ro% reached up to 3.60% in Jiaoshiba area or even higher of 3.92% in Taiyang area, the hydrogen isotopic trend is negative between methane and ethane, i.e., $\delta^2H_1 > \delta^2H_2$. The magnitude of hydrogen isotopic reversal is the biggest in the Pengshui area (up to 54‰). This implies that the change of hydrogen isotopic value of ethane is similar to that of the carbon isotope of ethane and propane, i.e., with increasing thermal maturity, ethane first becomes more enriched in D (positive trend), then becomes more depleted in D (negative trend), and finally becomes enriched in D again with increasing thermal maturity. During this maturation process, the hydrogen isotopic difference between methane and ethane becomes bigger and bigger, then gets smaller and smaller. The turning point occurs in the gases from Pengshui area with Ro% of 3.20%. Though the hydrogen isotopic difference between methane and ethane gets smaller and smaller, gases from Taiyang gas field still demonstrate a negative trend of hydrogen isotopic composition between methane and ethane ($\delta^2H_1 > \delta^2H_2$). Compared to the carbon isotopic values of ethane with increasing thermal maturity, there is an apparent delay in the changes of hydrogen isotopic values of ethane with increasing thermal maturity. For example, compared to the negative trend of carbon isotope ($\delta^{13}C_1 > \delta^{13}C_2$) in all gas samples, the hydrogen isotopic distribution pattern is still positive in the Weirong and Yongchuan areas at relatively lower thermal maturity, and it becomes negative with increasing thermal maturity. This clearly indicates the influences from the water salinity of the depositional environment. Due to the strong influences from the water salinity, similar to methane, ethane should have similar hydrogen isotopic compositions of gases from these areas, and hydrogen isotopic distribution trend between ethane and propane should be positive. With increasing thermal maturity, due to the relatively small amount of ethane, mixing effects with D-depleted products will be more important and result in the depletion of D in ethane, causing the reversed hydrogen isotopic distribution pattern between methane and ethane ($\delta^2H_1 > \delta^2H_2$).

Though Fig. 9 displays that all gas samples from Taiyang, Jiaoshiba and Weirong gas fields are characterized by $\delta^{13}C_1 > \delta^{13}C_2$, in general, with increasing thermal maturity (or decreasing gas wetness), methane become more enriched in ^{13}C throughout the whole process (Fig. 10a), while ethane first become more enriched in ^{13}C, then become more depleted in ^{13}C, and finally become more enriched in ^{13}C again (Fig. 10b) (Burruss and Laughrey, 2010; Dai et al., 2014, 2016, 2017; Feng et al., 2020; Ferworn et al., 2008; Hao and Zou, 2013; Liu et al., 2018; Ni et al., 2018a; Rodriguez and Philp, 2010; Tilley and Muehlenbachs, 2013; Xia and Gao, 2018; Zumberge et al., 2012). Gas samples from the Weirong shale gas field, Fushun-Yongchuan area and the Weiyuan national shale gas demonstration zone mainly fall on the $\delta^{13}C_1$-wetness trendline, implying the controlling effects from thermal maturity, while the offset of gas samples from Taiyang and Jiaoshiba gas fields, Fuling and Changning-Zhaotong national shale gas demonstration zones may indicate the importance of the diffusive migration influences. Besides some small differences, changes of δ^2H_1 and δ^2H_2 values toward wetness have similar pattern to that of $\delta^{13}C_1$ and $\delta^{13}C_2$

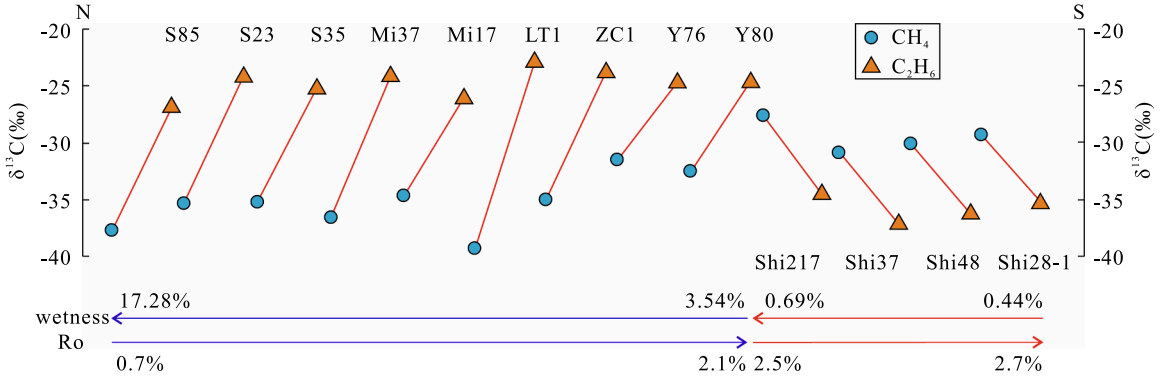

Fig. 8. Carbon isotopic distribution pattern between methane and ethane of natural gases from the Ordos Basin. Modified from Dai et al. (2017).

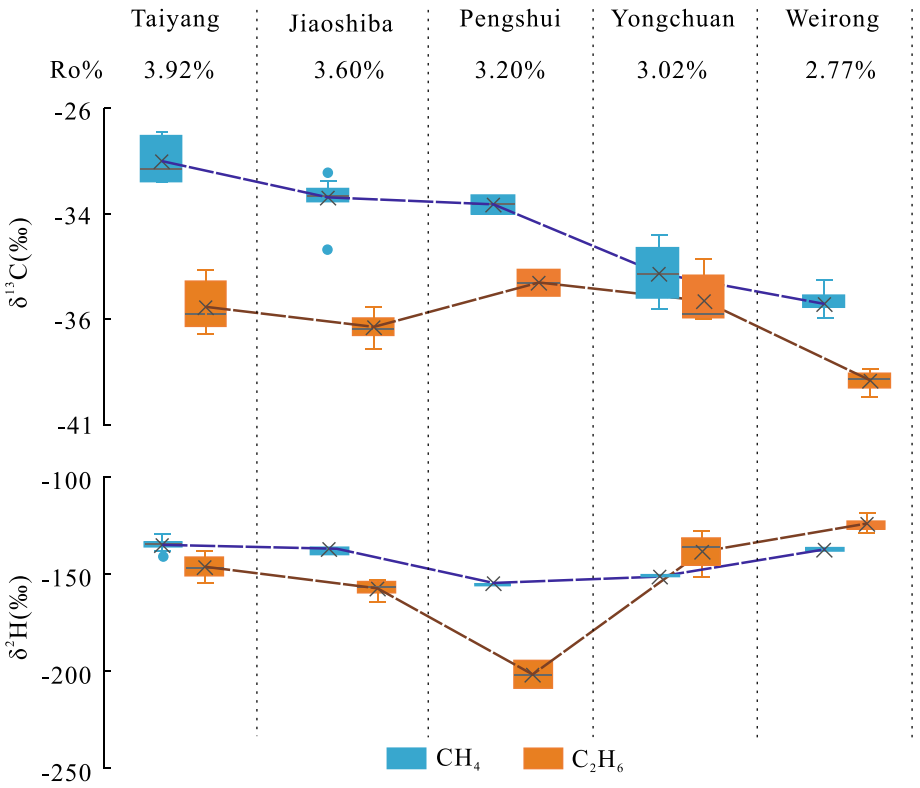

Fig. 9. Box plot of the stable carbon and hydrogen isotopic compositions of shale gases from Taiyang, Jiaoshiba, Weirong, Pengshui and Yongchuan areas.

values, respectively on the macroscopic scale. For the δ^2H_1 values, when wetness is > 8%, δ^2H_1 values increase with decreasing wetness rapidly, while when wetness is < 8%, the variation of the δ^2H_1 is very small and mainly in the range of (-140 ± 15)‰, indicating the strong influences from cogenetic water. With decreasing gas wetness (or increasing gas maturity), ethane first become more enriched in D and ^{13}C (i.e., increasing δ^2H_2 and $\delta^{13}C_2$ values with decreasing gas wetness), then become more depleted in D and ^{13}C (i.e., decreasing δ^2H_2 and $\delta^{13}C_2$ values with decreasing gas wetness), and finally become more enriched in D and ^{13}C again (i.e., increasing δ^2H_2 and $\delta^{13}C_2$ values with decreasing gas wetness) (Fig. 10b,d). The major difference between $\delta^{13}C_2$ and δ^2H_2 values is that the turning point of wetness from rollover zone to post-rollover zone is 1.2% for the $\delta^{13}C_2$ value while 0.8% for the δ^2H_2 value. Such delay in hydrogen isotopic composition of ethane indicates the strong influences from the cogenetic water medium.

6. Conclusions

To date shale gas exploration have been carried out mainly in the Upper Ordovician Wufeng-Lower Silurian Longmaxi formations with burial depth mostly of 2000 ~ 3500 m in the only commercial shale gas producing basin—Sichuan Basin in China. This study investigated the hydrogen isotopic compositions of shale gases from the Wufeng- Longmaxi shale in the Taiyang, Jiaoshiba and Weirong shale gas fields in the southern Sichuan Basin. The burial depths are < 2250 m in the Taiyang shale gas field, 2250 ~ 3500 m in the Jiaoshiba shale gas field and > 3500 m in the Weirong shale gas field. Shale gases from the Taiyang, Jiaoshiba and Weirong gas fields have average δ^2H_1 and δ^2H_2 values of −135‰ and −146‰ (n = 10), of −137‰ and −157‰ (n = 10), and of −137‰ and −124‰ (n = 11), respectively, and average $\delta^{13}C_1$, $\delta^{13}C_2$ and $\delta^{13}C_3$ values of −28.5‰, −35.4‰ and −36.2‰ (n = 10), of −30.3‰, −36.4‰ and −38.4‰ (n = 10), and of −35.2‰, −38.9‰ and −40.8‰ (n = 11), respectively. When thermal maturity increased from 2.77% in Weirong shale gas field to 3.92% in Taiyang shale gas field, the δ^2H_1 values are similar in the Taiyang, Jiaoshiba and Weirong shale gas fields with an average value ranging from −135‰ to −137‰, while the δ^2H_2 values varies greatly, with an average of −124‰, −157‰ and −146‰ in Weirong, Jiaoshiba and Taiyang, respectively. Generally, it is found that when wetness > 8%, δ^2H_1 values increase with decreasing wetness rapidly demonstrating the dominant influences from thermal maturity, while when wetness < 8%, the variation of the δ^2H_1 values is mainly in the range of (-140 ± 15)‰, indicating the strong influences from cogenetic water. The hydrogen isotopic distribution pattern between methane and ethane is positive trend ($\delta^2H_1 < \delta^2H_2$) in the Weirong shale gas field, but with increasing thermal maturity, it changes into negative trend ($\delta^2H_1 > \delta^2H_2$) in the Jiaoshiba and Taiyang shale gas fields. This implies that the hydrogen isotopic composition of shale gas is largely affected by the cogenetic water. Generally, with decreasing gas wetness, ethane first become more enriched in D and ^{13}C, then become more depleted in D and ^{13}C, and finally become more enriched in D and ^{13}C again. Though the δ^2H_2 values have similar evolution trend with that of the $\delta^{13}C_2$ values, there is a delay in the δ^2H_2 values. The turning point of wetness from rollover zone to post-rollover zone is 1.2% for the $\delta^{13}C_2$ value while 0.8% for the δ^2H_2 value. This may indicate hydrogen isotopic composition is influenced not only by the thermal maturity but also by the cogenetic water medium.

CRediT authorship contribution statement

Yunyan Ni: Conceptualization, Funding acquisition, Data curation, Writing – original draft, Writing – review & editing, Visualization. **Dazhong Dong:** Resources, Writing – original draft, Validation. **Limiao Yao:** Formal analysis, Methodology, Visualization. **Jianping Chen:** Data curation, Validation. **Jianli Sui:** Formal analysis, Methodology, Data curation. **Fei Wang:** Data curation, Investigation. **Fei Liu:** Data curation, Investigation. **Jian Li:** Data curation, Validation. **Jinhao Guo:** Formal analysis, Methodology. **Dan Liu:** Validation, Investigation, Visualization. **Jinliang Gao:** Validation, Investigation, Visualization.

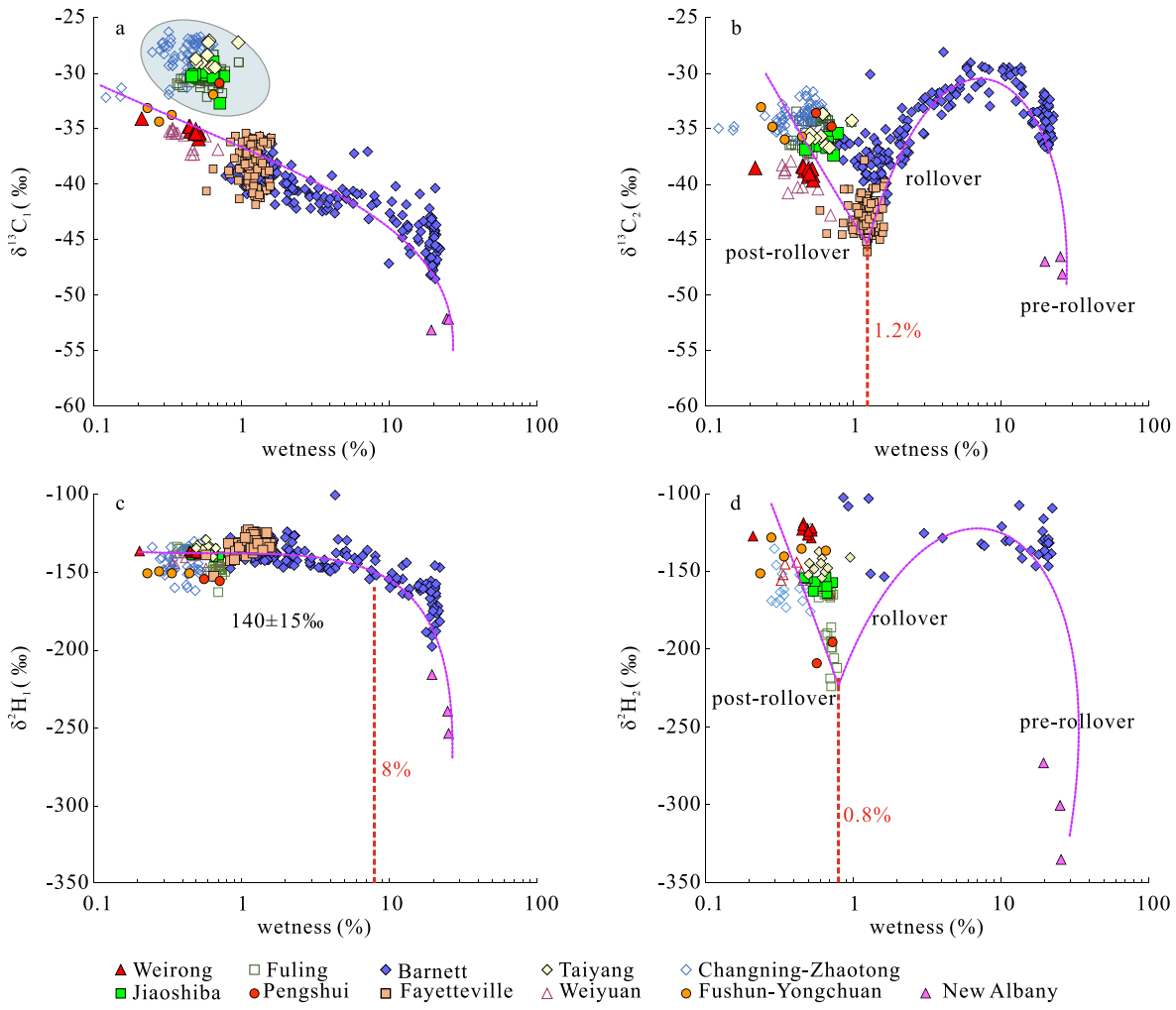

Fig. 10. Plots of wetness versus $\delta^{13}C_1$ (a), $\delta^{13}C_2$ (b), $\delta^{2}H_1$ (c) and $\delta^{2}H_2$ of shale gases from Taiyang, Jiaoshiba and Weirong gas fields. Also shown are shale gases from the published data (Cao et al., 2020; Chen et al., 2020; Dai et al., 2016; Feng et al., 2019, 2020; Rodriguez and Philp, 2010; Strąpoć et al., 2010; Zhang et al., 2018; Zumberge et al., 2012).

Declaration of Competing Interest

The authors declare the following financial interests/personal relationships which may be considered as potential competing interests: Authors Fei Liu and Fei Wang are employed by PetroChina Zhejiang Oilfield Company. The remaining authors declare that the research was conducted in the absence of any commercial or financial relationships that could be construed as a potential conflict of interest.

Data availability

No data was used for the research described in the article.

Acknowledgments

We thank Prof. Jinxing Dai from the PetroChina Research Institute of Petroleum Exploration and Development for helpful discussion. This study is funded by the National Key Research and Development Projects of China (Grant No. 2019YFC1805505) and the PetroChina Scientific Research and Technology Development Project (Grant No. 2021DJ05, 2021DJ5302).

Authors Fei Wang and Fei Liu are employed by PetroChina Zhejiang Oilfield Company. The remaining authors declare that the research was conducted in the absence of any commercial or financial relationships that could be construed as a potential conflict of interest.

References

Barker, L.F., 1984. The geochemistry and origin of natural gases in Southern Ontario. Bull. Can. Pet. Geol. 32, 313–326.

Behar, F., Vandenbroucke, M., Teermann, S.C., Hatcher, P.G., Leblond, C., Lerat, O., 1995. Experimental simulation of gas generation from coals and a marine kerogen. Chem. Geol. 126 (3-4), 247–260.

Berner, U., Faber, E., 1996. Empirical carbon isotope/maturity relationships for gases from algal kerogens and terrigenous organic matter, based on dry, open-system pyrolysis. Org Geochem. 24 (10-11), 947–955.

Bottinga, Y., 1969. Calculated fractionation factors for carbon and hydrogen isotope exchange in the system calcite-carbon dioxide-graphite-methane-hydrogen-water vapor. Geochim. Cosmochim. Acta 33 (1), 49–64.

Burruss, R.C., Laughrey, C.D., 2010. Carbon and hydrogen isotopic reversals in deep basin gas: Evidence for limits to the stability of hydrocarbons. Org Geochem. 41 (12), 1285–1296.

Cao, C., Zhang, M., Li, L., Wang, Y., Li, Z., Du, L.i., Holland, G., Zhou, Z., 2020. Tracing the sources and evolution processes of shale gas by coupling stable (C, H) and noble gas isotopic compositions: Cases from Weiyuan and Changning in Sichuan Basin, China. J. Nat. Gas. Sci. Eng. 78, 103304.

Chen, Z., Chen, L., Wang, G., Zou, C., Jiang, S., Si, Z., Gao, W., 2020. Applying isotopic geochemical proxy for gas content prediction of Longmaxi shale in the Sichuan Basin, China. Mar. Petrol. Geol. 116, 104329.

Chen, J., Li, C., Shen, P., Ying, G., 1995. Carbon and hydrogen isotopic characteristics of hydrocarbons in coal type gas from China. Sedimentologica Sinica 13, 59–69.

Chen, J., Wang, X., Chen, J., Ni, Y., Xiang, B., He, W., Yao, L., Li, E., 2021. New formula to decipher the relationship between carbon isotope composition of methane and maturity of natural gas source rocks. Sci. China (Earth Sci.) 64 (3), 470–493.

Chung, H.M., Gormly, J.R., Squires, R.M., 1988. Origin of gaseous hydrocarbons in subsurface environment: theoretical considerations of carbon isotope distribution. Chem. Geol. 71, 97–103.

Curtis, J.B., 2002. Fractured Shale-Gas Systems. AAPG Bull. 86, 1921–1938.

Dai, J., 1993. Characteristics of carbon and hydrogen isotopes of natural gases and their discriminations. Nat. Gas Geosci. 1–40.
Dai, J., Li, J., Luo, X., Zhang, W., Hu, G., Ma, C., Guo, J., Ge, S., 2005. Stable carbon isotope compositions and source rock geochemistry of the giant gas accumulations in the Ordos Basin, China. Org. Geochem. 36 (12), 1617–1635.
Dai, J., Ni, Y., Zou, C., 2012a. Stable carbon and hydrogen isotopes of natural gases sourced from the Xujiahe Formation in the Sichuan Basin, China. Org. Geochem. 43, 103–111.
Dai, J., Xia, X., Li, Z., Coleman, D.D., Dias, R.F., Gao, L., Li, J., Deev, A., Li, J., Dessort, D., Duclerc, D., Li, L., Liu, J., Schloemer, S., Zhang, W., Ni, Y., Hu, G., Wang, X., Tang, Y., 2012b. Inter-laboratory calibration of natural gas round robins for δ^2H and $\delta^{13}C$ using off-line and on-line techniques. Chem. Geol. 310–311, 49–55.
Dai, J., Zou, C., Liao, S., Dong, D., Ni, Y., Huang, J., Wu, W., Gong, D., Huang, S., Hu, G., 2014. Geochemistry of the extremely high thermal maturity Longmaxi shale gas, southern Sichuan Basin. Org Geochem. 74, 3–12.
Dai, J., Zou, C., Dong, D., Ni, Y., Wu, W., Gong, D., Wang, Y., Huang, S., Huang, J., Fang, C., Liu, D., 2016. Geochemical characteristics of marine and terrestrial shale gas in China. Mar. Petrol. Geol. 76, 444–463.
Dai, J., Ni, Y., Gong, D., Feng, Z., Liu, D., Peng, W., Han, W., 2017. Geochemical characteristics of gases from the largest tight sand gas field (Sulige) and shale gas field (Fuling) in China. Mar. Petrol. Geol. 79, 426–438.
Feng, Z., Dong, D., Tian, J., Wu, W., Cai, Y., Shi, Z., Peng, W., 2019. Geochemical characteristics of Lower Silurian shale gas in the Changning-Zhaotong exploration blocks, southern periphery of the Sichuan Basin. J. Pet. Sci. Eng. 174, 281–290.
Feng, Z., Hao, F., Dong, D., Zhou, S., Wu, W., Xie, C., Cai, Y., Li, Z., 2020. Geochemical anomalies in the Lower Silurian shale gas from the Sichuan Basin, China: Insights from a Rayleigh-type fractionation model. Org Geochem 142, 103981.
Ferworn, K., Zumberge, J., Reed, J., Brown, S., 2008. Gas character anomalies found in highly productive shale gas wells. http://www.zenzebra.net/quebec/Ferworn_et_al_2008.pdf.
Gao, L., Schimmelmann, A., Tang, Y., Mastalerz, M., 2014. Isotope rollover in shale gas observed in laboratory pyrolysis experiments: Insight to the role of water in thermogenesis of mature gas. Org Geochem. 68, 95–106.
Hao, F., Zou, H., 2013. Cause of shale gas geochemical anomalies and mechanisms for gas enrichment and depletion in high-maturity shales. Mar. Petrol. Geol. 44, 1–12.
Huang, S., Duan, S., Wang, Z., Jiang, Q., Jiang, H., Su, W., Qingfu, F., Huang, T., Yuan, M., Ren, M., Chen, X., 2019. Affecting factors and application of the stable hydrogen isotopes of alkane gases. Petrol. Explor. Develop. 46 (3), 518–530.
Jenden, P.D., Drazan, D.J., Kaplan, I.R., 1993. Mixing of thermogenic natural gases in northern Appalachian Basin. AAPG Bull. 77, 980–998.
Liang, X., Xu, Z., Zhang, J., Zhang, Z., Li, Z., Jiang, P., Jiang, L., Zhu, D., Liu, C., 2020. Key efficient exploration and development technologies of shallow shale gas: a case study of Taiyang anticline area of Zhaotong National Shale Gas Demonstration Zone. Acta Petrol. Sin. 41, 1033–1048.
Liang, X., Shan, C., Zhang, Z., Xu, J., Wang, W., Zhang, J., Xu, Y., 2021. "Three-dimensional closed system" accumulation model of Taiyang anticline mountain shallow shale gas in Zhaotong demonstration area. Acta Geol. Sin. 95, 1–20.
Liu, Q., Jin, Z., Wang, X., Yi, J., Meng, Q., Wu, X., Gao, B., Nie, H., Zhu, D., 2018. Distinguishing kerogen and oil cracked shale gas using H, C-isotopic fractionation of alkane gases. Mar. Petrol. Geol. 91, 350–362.
Liu, Q.Y., Wu, X.Q., Wang, X.F., Jin, Z.J., Zhu, D.Y., Meng, Q.Q., Huang, S.P., Liu, J.Y., Fu, Q., 2019. Carbon and hydrogen isotopes of methane, ethane, and propane: A review of genetic identification of natural gas. Earth Sci. Rev. 190, 247–272.
Lorant, F., Prinzhofer, A., Behar, F., Huc, A.-Y., 1998. Carbon isotopic and molecular constraints on the formation and the expulsion of thermogenic hydrocarbon gases. Chem. Geol. 147 (3-4), 249–264.
Ni, Y.Y., Dai, J.X., Zhu, G.Y., Zhang, S.C., Zhang, D.J., Su, J., Tao, X.W., Liao, F.R., Wu, W., Gong, D.Y., Liu, Q.Y., 2013. Stable hydrogen and carbon isotopic ratios of coal-derived and oil-derived gases: A case study in the Tarim basin, NW China. Int. J. Coal Geol. 116–117, 302–313.
Ni, Y.Y., Zhang, D.J., Liao, F.R., Gong, D.Y., Xue, P., Yu, F., Yu, J.Z.C., Ping, J., Zhao, C. Y., Hu, J., Jin, Y., 2015. Stable hydrogen and carbon isotopic ratios of coal-derived gases from the Turpan-Hami Basin, NW China. Int. J. Coal Geol. 152, 144–155.
Ni, Y.Y., Gao, J.L., Chen, J.P., Liao, F.R., Liu, J.Q., Zhang, D.J., 2018a. Gas generation and its isotope composition during coal pyrolysis: Potential mechanism of isotope rollover. Fuel 231, 387–395.
Ni, Y.Y., Liao, F.R., Gao, J.L., Chen, J.P., Yao, L.M., Zhang, D.J., 2019. Hydrogen isotopes of hydrocarbon gases from different organic facies of the Zhongba gas field, Sichuan Basin, China. J. Pet. Sci. Eng. 179, 776–786.
Ni, Y.Y., Dong, D.Z., Yao, L.M., Chen, J.P., Liang, X., Liu, F., Li, J., Guo, J., Gao, J.L., 2022a. Geochemical characteristics and origin of shale gases from Sichuan Basin, China. Front. Earth Sci. 10, 884445.
Ni, Y., Ma, Q., Ellis, G.S., Dai, J., Katz, B., Zhang, S., Tang, Y., 2011. Fundamental studies on kinetic isotope effect (KIE) of hydrogen isotope fractionation in natural gas systems. Geochim. Cosmochim. Acta 75 (10), 2696–2707.
Ni, Y.Y., Yao, L.M., Sui, J.L., Chen, J.P., 2022b. Isotopic geochemical characteristics and identification indexes of shale gas hydraulic fracturing flowback water/produced water. J. Nat. Gas Geosci. 33, 78–91.
Ni, Y., Zou, C., Cui, H., Li, J., Lauer, N.E., Harkness, J.S., Kondash, A.J., Coyte, R.M., Dwyer, G.S., Liu, D., Dong, D., Liao, F., Vengosh, A., 2018b. The origin of flowback and produced waters from Sichuan Basin, China. Environ. Sci. Technol. 52 (24), 14519–14527.
Pernaton, E., Prinzhofer, A., Schneider, F., 1996. Reconsideration of methane isotope signature as a criterion for the genesis of natural gas: influence of migration on isotopic signatures. Revue de l'Institut Francais du Petrole 51 (5), 635–651.
Reeves, E.P., Seewald, J.S., Sylva, S.P., 2012. Hydrogen isotope exchange between n-alkanes and water under hydrothermal conditions. Geochim. Cosmochim. Acta 77, 582–599.
Rodriguez, N.D., Philp, R.P., 2010. Geochemical characterization of gases from the Mississippian Barnett Shale, Fort Worth Basin, Texas. AAPG Bull. 94 (11), 1641–1656.
Rooney, M.A., Claypool, G.E., Moses Chung, H., 1995. Modeling thermogenic gas generation using carbon isotope ratios of natural gas hydrocarbons. Chem Geol. 126 (3-4), 219–232.
Schimmelmann, A., Sessions, A.L., Mastalerz, M., 2006. Hydrogen isotopic (D/H) composition of organic matter during diagenesis and thermal maturation. Annu. Rev. Earth Planet. Sci. 34 (1), 501–533.
Schoell, M., 1980. The hydrogen and carbon isotopic composition of methane from natural gases of various origins. Geochim Cosmochim. Acta 44 (5), 649–661.
Stahl, W.J., 1977. Carbon and nitrogen isotopes in hydrocarbon research and exploration. Chem. Geol. 20, 121–149.
Stahl, W.J., Carey, B.D., 1975. Source-rock identification by isotope analyses of natural gases from fields in the Val Verde and Delaware basins, West Texas. Chem. Geol. 16 (4), 257–267.
Strąpoć, D., Mastalerz, M., Schimmelmann, A., Drobniak, A., Hasenmueller, N.R., 2010. Geochemical constraints on the origin and volume of gas in the New Albany Shale (Devonian–Mississippian), eastern Illinois Basin. AAPG Bull. 94 (11), 1713–1740.
Tang, Y., Perry, J.K., Jenden, P.D., Schoell, M., 2000. Mathematical modeling of stable carbon isotope ratios in natural gases. Geochim. Cosmochim. Acta 64 (15), 2673–2687.
Tang, Y., Huang, Y., Ellis, G.S., Wang, Y.i., Kralert, P.G., Gillaizeau, B., Ma, Q., Hwang, R., 2005. A kinetic model for thermally induced hydrogen and carbon isotope fractionation of individual n-alkanes in crude oil. Geochim. Cosmochim. Acta 69 (18), 4505–4520.
Tenger, B., Shen, B.J., Yu, L.J., Yang, Y.F., Zhang, W.T., Tao, C., Xi, B.B., Zhang, Q.Z., Bao, F., Qin, J.Z., 2017. Mechanism of shale gas generation and accumulation in the Ordovician Wufeng-Longmaxi Formation, Sichuan Basin, SW China. Petrol. Explor. Develop. 44, 69–78.
Tilley, B., Muehlenbachs, K., 2013. Isotope reversals and universal stages and trends of gas maturation in sealed, self-contained petroleum systems. Chem. Geol. 339, 194–204.
Vengosh, A., Jackson, R.B., Warner, N., Darrah, T.H., Kondash, A., 2014. A critical review of the risks to water resources from unconventional shale gas development and hydraulic fracturing in the United States. Environ. Sci. Tech. 48 (15), 8334–8348.
Wang, Y.M., Chen, B., Li, X.J., Wang, H., Chang, L.C., Jiang, S., 2018. Sedimentary characteristics of upwelling facies shale in Lower Silurian Longmaxi Formation, northeast Sichuan area. Acta Petrol. Sin. 39, 1092–1102.
Wang, Y., Qiu, N.S., Yang, Y.F., Rui, X.Q., Zhou, Y.Y., Fang, G.J., Wu, H., Shen, B.J., Cheng, L.J., 2019. Thermal maturity of Wufeng-Longmaxi shale in Sichuan Basin. Earth Sci. 44, 953–971.
Wang, X., Liu, W., Shi, B., Zhang, Z., Xu, Y., Zheng, J., 2015a. Hydrogen isotope characteristics of thermogenic methane in Chinese sedimentary basins. Org Geochem. 83–84, 178–189.
Wang, Y.M., Zhong, D.D., Li, X.J., Liang, H.J., Wang, H.F., Wu, W., 2015b. Stratigraphic sequence and sedimentary characteristics of Lower Silurian Longmaxi Formation in the Sichuan Basin and its peripheral areas. Nat. Gas Ind. 35, 12–21.
Xia, X., Chen, J., Braun, R., Tang, Y., 2013. Isotopic reversals with respect to maturity trends due to mixing of primary and secondary products in source rocks. Chem. Geol. 339, 205–212.
Xia, X., Gao, Y., 2017. Mechanism of linear covariations between isotopic compositions of natural gaseous hydrocarbons. Org Geochem. 113, 115–123.
Xia, X., Gao, Y., 2018. Depletion of ^{13}C in residual ethane and propane during thermal decomposition in sedimentary basins. Org Geochem. 125, 121–128.
Zhang, T., Krooss, B.M., 2001. Experimental investigation on the carbon isotope fractionation of methane during gas migration by diffusion through sedimentary rocks at elevated temperature and pressure. Geochim. Cosmochim. Acta 65 (16), 2723–2742.
Zhang, M., Tang, Q., Cao, C., Lv, Z., Zhang, T., Zhang, D., Li, Z., Du, L., 2018. Molecular and carbon isotopic variation in 3.5 years shale gas production from Longmaxi Formation in Sichuan Basin, China. Mar. Petrol. Geol. 89, 27–37.
Zhu, C.Q., Hu, S.B., Qiu, N.S., Rao, S., Yuan, Y.S., 2016. Thermal history of the Sichuan Basin, SW China: Evidence from deep boreholesn. Sci. China (Earth Sci.) 59, 70–82.
Zou, C.N., Zhao, Q., Cong, L.Z., Wang, H.Y., Shi, Z.S., Wu, J., Pan, S.Q., 2021. Development progress, potential and prospect of shale gas in China. Nat. Gas Ind. 41, 1–14.
Zumberge, J., Ferworn, K., Brown, S., 2012. Isotopic reversal ('rollover') in shale gases produced from the Mississippian Barnett and Fayetteville formations. Mar. Petrol. Geol. 31 (1), 43–52.